

LLDPE's grown with Metallocene and Ziegler–Natta catalysts: events in the melt and FTIR analysis

Z. Ferhat-Hamida · H. Phuong-Nguyen ·
P. Bernazzani · A. Haine · G. Delmas

Received: 29 June 2004 / Accepted: 17 August 2006 / Published online: 29 March 2007
© Springer Science+Business Media, LLC 2007

Abstract LLDPE samples synthesized with Ziegler–Natta (ZN) and Metallocene (MT) catalysts have been analyzed to investigate a potential catalyst-dependent morphology and to find an explanation for the difficult processing of MT. Slow calorimetry at $\nu = 0.02$ K/min and IR at RT and in the melt are used. The differences between MT and ZN are assigned to their different composition, MT not having the linear segments, which are present in ZN. Slow calorimetry is effectively a drawing process of the melt with chain orientation followed by decay. The later event, characterized by an endotherm, $\Delta H_{\text{network}}$, occurs at higher temperatures for MT, the presence of a regular distribution of methyl groups slowing down the process. The rocking, gauche, bending and stretching regions of the IR spectra are analyzed. The nascent MT has more strained bands in the rocking region. The wagging region reveals the more homogeneous environment of MT through the maximum absorbance at $1,368\text{ cm}^{-1}$. Decomposition of bands is made for the rocking and wagging regions. The orthorhombic crystallinity, α_c (FTIR), measures the sum of long- and short-range orthorhombic order, the latter being obtained by α_c (FTIR)- α_c (X-rays). The values of α_c (FTIR) for MT and ZN are very similar in conditions of equilibrium. The justifications for the molecular origin

of $\Delta H_{\text{network}}$ are presented: (i) the slow relaxation of long chains strained and oriented in the melt measured by other techniques, (ii) The correlation, for gels of a linear sample, made in different solvents, between the maximum drawability, λ_{max} , and $\Delta H_{\text{network}}$ in a slow T -ramp. The range is 80–270 for λ_{max} and 40–120 J/g for $\Delta H_{\text{network}}$. (iii) The comparison of two traces of the same sample, between 140 °C and 270 °C, show that comparable events in the melt appear in the integrated absorbance and in the slow calorimetry signal. Analysis on thin films of the little-studied CH_2 stretching region reveals that their extinction coefficient, ε , and the shape of the bands are highly sensitive to the sample history, ε diminishing by a large factor in slowly crystallized samples. Events in the slow T -ramp, followed by a fast crystallization, on the other hand, leads to materials with standard characteristics. Slow calorimetry traces display more events (endothermic and exothermic) for MT than for ZN, a finding consistent with more flow irregularities during processing. Equilibrium conditions and better processing could be reached for MT by extending time in the melt or using higher temperatures.

Z. Ferhat-Hamida · H. Phuong-Nguyen ·
A. Haine · G. Delmas (✉)
Chemistry Department, Université du Québec in Montréal,
CP 8888, Succ Centre ville, Montreal, Canada H3C 3P8
e-mail: delmas-patterson.genevieve@uqam.ca

P. Bernazzani
Chemical Engineering Department, Texas Tech University,
Lubbock, TX 79409-3121, USA

Introduction

The two-phase model of a semi-crystalline polymer is consistent with the calorimetry and X-ray techniques, which permit the characterization of the crystalline and amorphous phases of these materials. However, other techniques such as ^{13}C NMR [1, 2], Raman [3], slow calorimetry and FTIR reveal the existence of regions

whose organization or mobility is intermediary between that of the crystalline and amorphous phases. The name of the other morphology depends somewhat on the technique used for its characterization. The fraction is interfacial in Raman or ^{13}C NMR research and network-like in slow calorimetry [4–13] and FTIR [14–17] work. The term network is suited to describe an assembly of entangled chains whose junctions are branches and knots. These knots lead to short-range order between the chains rather than tri-dimensional long-range order. FTIR spectra reveal that the network fraction is part of both the orthorhombic fraction and the amorphous phase. Slow calorimetry traces display two endotherms for PE as solid, solutions or gels and for a variety of polymers. The low- T one corresponds to the cooperative melting/dissolution seen by fast DSC and the high- T one, with a slower kinetics, has been attributed to the melting/dissolution of strained order (see Appendix 1). Slow relaxation of oriented chains seems now a suitable origin of the second endotherm since it explains well some experimental data as presented below.

The fast kinetics of melting/dissolution of long-range order in a rapid T -ramp has been followed by X-ray diffraction or DSC. However, above T_m , due to the slow kinetics of chain randomization, the melt is rather heterogeneous or semi-ordered. Birefringence in PE melt has been shown to be resistant to decay [18]. Early work on calorimetry of hydrogen-bonded materials had recognized the effect of the rate of heating on the characteristics of melting. The value of $\Delta H_{\text{melting}}$ as measured by DSC in those systems was found to vary considerably with the heating rate [18]. Calorimetric traces of amylose + water mixtures [12, 13] and IR spectra [17] are sensitive to sample history and rate of heating. Although the effect of knots on chain mobility was acknowledged in the literature, the concept of strain building in entangled polymers during a rapid temperature ramp has been used only recently [4–13]. Several groups have investigated the presence of order in amorphous polymers or in the melt of crystallizable polymers by a variety of techniques [19]. Research on PE has used ^{13}C NMR [20–21], rheology [22], hypersonic properties [23] and slow calorimetry [4–13]. Events in the melt of linear PE have been observed recently [24] by mechanical properties and DSC traces but no value of the enthalpy accompanying them is given.

Linear Low density PE resins (LLDPE) have been synthesized from ethylene and a longer alkene by heterogeneous Ziegler–Natta catalysts (ZN) but a new technique using Metallocene catalysts (MT) has been developed. Since the new products are different in extrusion, analysis of their melt by calorimetry and other techniques seems appropriate to understand the origin of the difference. Results in the literature [25–29] and in

this laboratory [30] suggest that it is more the response to strain/orientation which is important and possibly catalyst-specific than the morphology in equilibrium conditions. The comparison of two LLDPE, called simply MT and ZN, analyzed by a variety of standard techniques, by slow calorimetry and by FTIR is presented. The little-studied CH_2 stretching vibrations lead to new results from thin films crystallized from the melt at different rates of cooling.

Materials and equipment

Materials

The samples are commercial Bayer samples received as nascent materials without additives from Sarnia, Ont. Canada. They are called MT and ZN to refer to the Metallocene and Ziegler–Natta catalysts used for their synthesis. The characteristics of MT and ZN are listed in Table 1. They were taken on samples aged for less than four months. Films for FTIR prepared in solution are S-films and those prepared with the press are P-films. Calorimetric and FTIR data are reported also for a low MW linear Union Carbide sample, MI37, ($d=0.96\text{ g/cm}^3$ for a S-film, $M_w = 35,000$ and $MI = 37$). Calorimetric results are mentioned for a low MW standard PE MS2 [31] ($d = 0.96\text{ g/cm}^3$, $M_w = 5.800$ and $M_w/M_n < 1.1$).

Apparatus

Calorimeters: Setaram C80. Slow calorimetry was performed with the sensitive and stable C80 Setaram calorimeter used in previous work [4–13]. The rate of heating, ν , is 0.02 K/min for MT and ZN and 0.05 K/min for MI37. Some measurements are taken with

Table 1 Characteristics of the MT and ZN samples^a

Sample	Density g/cm^3	$M_w \times 10^{-3}$ g/mol	M_w/M_n^b	$\text{CH}_2/1000\text{C}^c$	MI g/10 min
MT	0.92	150–200	2–3	17	1
ZN	0.92	150–200	3–4	14	1

^a MT (Metallocene), ZN (Ziegler–Natta). Polymer films made with the press at $T = T_m + (25\text{--}40\text{ K})$, 10–30 min under 21 metric ton

^b Using the LCST (Lower Critical Solution Temperature) technique³¹

^c Using the IR spectra and an empirical relationship

$\nu = 0.2$ K/min. The cooling rates varies between 0.1 K/min and 0.0167 K/min.

Above T_m , the maximum of the magnitude of the signal (0.060 mW) is about five times larger than the fluctuations [14] of the baseline (0.013) on the same temperature interval.

DSC : The DSC traces are obtained on a Du Pont and on a Perkin-Elmer apparatus run at 10 K/min.

FTIR: IR spectra were taken as previously [14–17] with a MB-series spectrometer (Bomen Inc., Quebec, Canada.) in transmission mode, at a resolution of 1 cm^{-1} and with 50 scans.

FTIR (T): The measurements were made on a home-made cell and the same IR apparatus. The sample and a thin thermocouple are placed between two AgCl disks maintained with Teflon tape. Teflon holds its mechanical properties up to 300 °C. The heating wires are plugged to a precise temperature controller. Aluminium foil surrounds the top and base of the cell. These wires emit IR radiation, which varies with the power. The signal from the cell has been measured in a blank experiment made at the same rate of heating and subtracted from the data with a sample. With $\nu = 0.05$ K/min, a spectra is taken every 3 K i.e., every 54 min, with an isothermal step during the spectra acquisition.

Density: Densities data were obtained with an Anton Paar quartz densitometer which measures the density of the liquid in which the solid sample has been equilibrated.

Solid state: ^{13}C NMR: CPMS spectra are taken in conditions similar to those previously reported [21]. The Chemagnetics CMX-300 spectrometer was operating at 75.3 MHz using a Chemagnetics PENCIL probe. The contact time was 3 ms. The spectra are obtained after 400 scans.

Procedures

Slow calorimetry

The sample for slow calorimetry (32 ± 3 mg) is placed with the substrate in a glass tube. The atmosphere is purged with N_2 for two hours before sealing. The substrate is either Hg (2.0 cm^3) or stainless steel powder. The ratio in weight of powder to sample is 100 as in [7]. Improvement of thermal contact between the sample and the cell through mixing with a conductive material had been found to lead to larger endotherms corresponding to more complete events in polypropylene melt [7]. The mechanism is not clear but is probably due to the combination of an increased heat conductivity and a

favourable substrate for crystallization. As a result, a succession of micro-steps of melting/recrystallization takes place in the sample. Integration of the signal between 150 °C and 280 °C gives $\Delta H_{\text{network}}$ which is often made of two parts. Reducing the sample mass increases also the conductivity across the sample [30]. Some FTIR spectra, taken with $m \approx 1$ mg after a slow heating/cooling cycle illustrate the effect on the bands of this long history.

Rerun: After a slow T -ramp, and a rapid or slow crystallization rate, a second melting at a fast rate leads to a main endotherm of melting where T_m and ΔH_m are as they are after a fast T -ramp. The change of T_m (2–4 K) is due to the loss of the nascent character of the sample and the reduced strain on the crystals during the second melting. In the UHMW sample, the diminution of T_m at the second melting is 6 K due to more strain in the high MW sample. The high- T endotherms of the recrystallized material are seen on the trace. The magnitude of $\Delta H_{\text{network}}$ in the second run, found higher with linear UHMWPE [5] than in the first run, is consistently lower for the LLDPE samples. This is possibly an effect of the higher temperature of evolution of $\Delta H_{\text{network}}$ in LLDPE.

FTIR analysis

Spectra are taken on P- or S-films or after a slow T -ramp on heating and cooling. The fine powder of nascent samples are analysed with an IR apparatus equipped with a micro-beam.

P-films: The conditions to obtain a film from the nascent sample suitable for FTIR analysis (thin and strain-free) were found by trial and errors and were different for the samples of different density [14]. The temperature of the press was $T_m + (25\text{--}40\text{ K})$, the duration of melting 10–30 min, the pressure 21 metric tons. A higher temperature of the press is matched with a shorter time of melting. With these conditions, the absorbances in polarized light were no different or little different (<10%) from those in unpolarized light.

S-films: Solutions of MT and ZN are prepared with $c = 1\text{--}2\%$ in different solvents. High boiling point solvents like decalin lead to higher α_c .

Films after slow calorimetry: The S-films and P-films prepared for the measurement of α_c are smooth and homogeneous. The thickness of the films, e , for the measurement of the extinction coefficient, ε , is easy to control. Measurements after slow calorimetry have been done under two conditions where the sample mass and ν_c (cooling) are different. When $m = 32$ mg and ν_c is 0.1 K/min, a thin

part of the material which crystallises as a ring against the glass tube is detached to take the spectra. Alternatively, a small amount of sample $m = 1$ mg is melted slowly on a KBr disk (placed in a glass tube) and cooled with $v_c = 0.0167$ K/min. The combination of a small mass and of a slower rate of crystallization does not modify the second melting trace but lead materials with an irregular thickness and regions with a lens-like appearance and to different IR spectra as reported in Part IV.

Comonomer content: The methyl content, x_{methyl} , is obtained from a standard empirical relationship on P-films and the ratio of two absorbances in the gauche or wagging region that at $1,378\text{ cm}^{-1}$, characteristic of a methyl group and that at $1,368\text{ cm}^{-1}$ used as a measure of the film thickness. $x_{\text{methyl}} = 27.9 (\text{Abs } 1378/\text{Abs } 1368) - 9.4$.

Spectral simulations: The value of α_c , the orthorhombic crystallinity is obtained through decomposition of the CH_2 rocking peaks through the following steps:

The spectra are baseline corrected and the absorbance zero is put at 800 cm^{-1} . Spectral simulations of the $775\text{--}675\text{ cm}^{-1}$ regions in the IR spectra are then performed using the software BGRAMS/386 by Galactic industries. The bands have a Gauss + Lorentz band shape, the widths at half height are 3.5 cm^{-1} for the orthorhombic peaks (730.6 cm^{-1} and 719.4 cm^{-1}), $10\text{--}16\text{ cm}^{-1}$ for the single chain band or amorphous region (725 cm^{-1}) and $15\text{--}19\text{ cm}^{-1}$ for the monoclinic-like peak (717 cm^{-1}). The area of the orthorhombic doublet is found easily without repeating the simulation. On the other hand, the decomposition of the non-orthorhombic phases into the amorphous and the monoclinic-like phase requires

several simulations to ensure reproducibility. In a few cases, some non-aged films can be simulated with only one non-orthorhombic phase.

Each fraction is calculated from the simulated spectra using Eq. (1) where the integrated absorbance of each band is rationed against the total area of the $775\text{--}675\text{ cm}^{-1}$ region. The integrated absorbance of the two peaks at 730.5 cm^{-1} and 719.4 cm^{-1} , both representing the orthorhombic fraction, are summed.

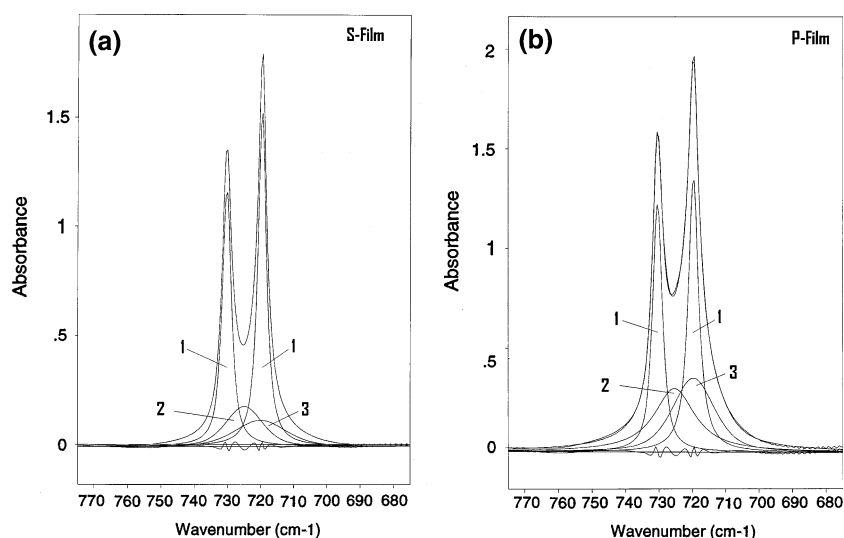
$$\alpha_{\text{phase},(i)} = \frac{\text{Integrated Area}_{\text{phase}(i)}}{\text{Integrated Area}_{\text{allthe phases}}} \quad (1)$$

The advantage of having three fractions rather than two in the rocking region is to keep the position of the amorphous fraction at about the same frequency $724 \pm 0.6\text{ cm}^{-1}$. With two bands, the position of the band is displaced of several cm^{-1} depending on the sample history. The position of the strained fraction i.e., of the monoclinic-like peak varies as it registers the strain in the sample and its history. A decomposition of the rocking region, similar to that of Fig. 1 is not given here for the nascent samples because of their variability from beads to beads and complexity and also because it requires more than four bands to achieve it.

Extinction coefficients ϵ : In the rocking region, the integrated absorbance is linear with e for thickness up to about $100\ \mu$ for films with the same history. The slope of the line gives ϵ with units of $\text{cm}^{-1}/e = \text{cm}^{-1}\ \mu^{-1}$.

The value of ϵ has been obtained for linear and branched PE films of different density. It varies between 0.34 and

Fig. 1 (a) The rocking region of a S-film showing the fraction of the crystalline (1), amorphous (2) and network (3) regions. (b) The rocking region of a P-film. Bands 2–3 reflect the lower values of α_c for the P-Films. No large difference is seen between the orthorhombic fractions MT and ZN with the same history (Table 2)



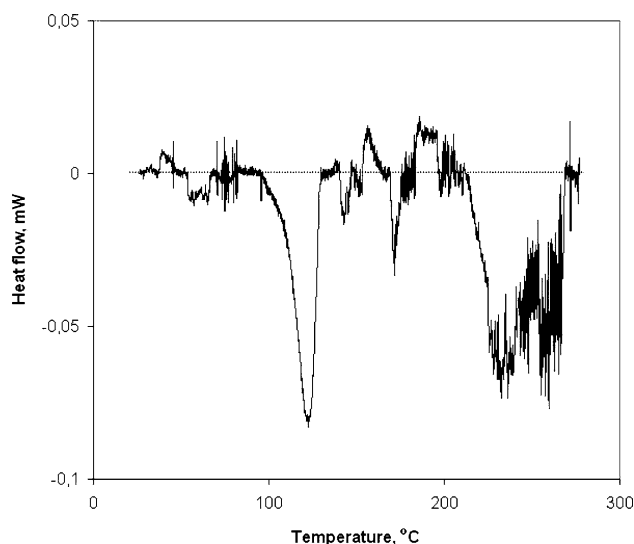


Fig. 2 Slow calorimetry trace of MT on a stainless steel substrate. $v = 0.02$ K/min. $m = 32.2$ mg. Weight ratio, substrate/sample ≈ 100

0.42 for $0.4 < \alpha_c < 0.8$. After correction for density, α/d increases. The calculation of the fraction of each fraction from the area of the peaks is exact if the extinction coefficient of the different fractions are the same. When the value of ε is corrected by the density, the ratio ε/d is found to vary with the sample crystallinity from 0.37 to 0.43 [14–15]. Equation (1) is still used without correction to calculate α_c because the change is not large and raw data are preferable for eventual use by a reader.

MW distribution

The values of M_w/M_n reported in Table 1, are obtained by fractionation at a Lower Critical Solution Temperature (LCST) in a volatile solvent. The solution is placed in a sealed glass tube and submitted to a step by step T increment. The highest MW's phase separate at lower temperatures. The set of h_i (T_i), h_i , being the turbidity peak evolved at T_i during phase separation leads to the MW distribution. Details on the constants used for linear and low density PE samples have been reported previously [31].

Results and discussion

The results for MT and ZN are presented under four different sections. In Part (I), the values of α_c , the crystallinity of samples submitted to different histories are given. Several standard techniques are used as well as a

quantitative IR analysis in the CH_2 rocking region. In Part (II), the traces of MT and ZN, obtained during a slow T -ramp (RT–270 °C) and the values of $\Delta H_{\text{network}}$ are compared. In Part (III), the molecular origin of $\Delta H_{\text{network}}$, consistent with the experimental results is presented. Support for the model comes from several data but from two in particular, namely the relationship between the maximum drawability λ_{max} and $\Delta H_{\text{network}}$ in gels and also from the comparison of IR spectra and calorimetric traces in the melt. In part (IV), the decomposition of the wagging region illustrates the advantages of band decomposition for a quantitative analysis of fractions. The spectra of non-treated and treated samples give an unexpected result on the sensitivity of the CH_2 stretching vibration to the sample history.

Part (I) Analysis of samples at RT

Samples of different crystallinity have been prepared and analyzed. Table 2 gives the values of α_c obtained by density (rows 1–4), X-ray (rows 5–7), DSC (rows 8–10) and NMR (rows 11, 12), for MT and ZN either nascent or for P- and S-films. The values of α_c (FTIR) calculated through the decomposition of the rocking region are presented (rows 13, 14).

Table 2 Values of the crystallinity α_c obtained by different techniques for nascent and recrystallized MT and ZN samples

α_c	History	MT	ZN
α_c (d)	Nascent	0.40	0.43
	P-film ^a	0.39	0.43
	S-film ^b	0.60	0.55
	S-film ^c	0.56–0.41	0.51–0.39
α_c (X-rays)	Nascent ^d	0.41	0.41
	P-film ^a	0.42	0.42
	S-film ^b	0.54	0.52
α_c (DSC)	Nascent	0.33	0.37
	P-film ^a	0.38	0.38
	S-film ^b	0.60	0.56
α_c (NMR)	Nascent ^d	0.65	0.63
	S-film ^{b,d}	0.74	0.71
α_c (FTIR)	P-film ^{a,e,f,g}	0.55 (0.20, 0.25)	0.58 (0.14, 0.28)
	S-film ^{b,e,f,g}	0.75 (0.12, 0.13)	0.72 (0.12, 0.16)

^a Films made with the press at $T = T_m + (25–40)$ K, 10–30 min, under 21 metric ton

^b Films prepared from solution (1% in toluene) $T_{\text{evap}} = \text{RT}$

^c Films prepared from solution (5% in toluene) $T_{\text{evap}} = \text{RT}$ to 116 °C

^d A small monoclinic fraction (0.02) is observed on the nascent sample by X-ray and ¹³C NMR

^e With e , thickness of the films such as $20 < e < 50$ μ

^f The fractions network and amorphous phases are in parenthesis

^g Average decomposition of 6 films

Crystallinity from density, X-rays, DSC and NMR

The different values of α_c (d) correspond to the nascent sample, to P-films (rows 1–2) and to S-films evaporated from a 1% solution (row 3). The 5% solution (row 4) has been evaporated at different temperatures (25–116 °C) to find out if the rate of crystallization was different for MT and ZN. The crystallinity decreases as the rate of solvent evaporation increases but is not significantly different for MT and ZN. Measurements on nascent samples are taken on non-aged materials.

The changes of the values of α_c (d) with crystallization conditions follow an expected trend. The P-films have about the same α_c as the nascent samples. The S-films have a higher crystallinity particularly those prepared from a 1% solution crystallized at room temperature in a solvent with a low volatility (α_c (d) = 0.60, 0.55). The difference in α_c between MT and ZN is not large but clear. It is due to the presence of some linear chains in ZN. MT has a lower crystallinity for a rapid crystallization (α_c = 0.39, 0.43) for the P-films but a higher crystallinity after dissolution and a slow crystallization (α_c = 0.60, 0.55 for the S-films). A slow growth from the melt leads to a different morphology from that of the S-films and a lower crystallinity [2] because the disentanglement is more complete in presence of a solvent. The values of α_c (DSC) is obtained, as for a linear PE, by the ratio, $\Delta H_{\text{melting}}/\Delta H_0$, ΔH_0 being the enthalpy of fusion of perfect crystals namely 293 J/g. For example, α_c (DSC) for the S-films is equal to 160–180/293.

The non-meltable long-range order is:

$$\alpha_{c \text{ non-meltable}} = \alpha_c (\text{X-rays}) - \alpha_c (\text{DSC}) \quad (2)$$

It is seen relatively large (0.08 for MT and 0.04 for ZN) in the nascent sample, which is entanglement-rich. The difference would be consistent with a larger network fraction in MT. However, since the two techniques have some degree of uncertainty, the non-meltable long-range order may be measurable only in special conditions.

The ^{13}C NMR spectrum separates the phases according to the mobility of the chains. Those participating in an organization (crystal or network) are less mobile than the free chains in the amorphous phase. Three phases have been identified by Horii et al. using ^{13}C NMR on linear PE and on LLDPE grown from Metallocene and Ziegler–Natta catalysts [2]. Although the methyl content of the LLDPE's investigated in [2] is lower than that of the present sample, the information contained in that research is worthwhile reporting. The interfacial phase of intermediate mobility is assumed to be comparable to our network fraction. Interesting features are shown by the comparison of MT and ZN: (i) the two fractions of restricted mobility are present in about the same amount. (ii) The mobile/rubbery fraction

is only 0.10. and (iii) the interfacial phase is more abundant for MT, 0.41 compared to 0.32. The characterization of the network fraction by slow calorimetry below, done in conditions very different from those of the ^{13}C NMR analysis, is nevertheless consistent with the ^{13}C NMR results at RT. The present ^{13}C NMR spectra have not been decomposed with three fractions because of the in-depth analysis developed in [2] and for simplicity. The spectra are decomposed instead with two (with peaks at 33.1 ppm and 30.7 ppm). It is to be noted that the values of α_c (NMR) found for the nascent (0.65, for MT, 0.63 for ZN) are higher than those found from d , X-rays and DSC (0.33–0.43). The physical cross-links, present in the network phase, reduce the chains mobility to a value comparable to those of the chains participating in long-range order. These cross-links are in higher concentration in the nascent than in the re-crystallized sample. In the S-films, α_c is also high due to the large fraction of orthorhombic order.

Crystallinity from the FTIR spectra

Assignment of IR PE bands was reported in the sixties and application to the measurements of crystallinity and tension in polyolefins [32–35] and hydrogen-bonded materials [17] followed. Deconvolution of bands and their change with sample history are now more reliable due to the improvement of IR techniques.

Long- and short- range orthorhombic order: The decomposition of two spectra is given in Fig. 1 for a S-film and a P-film. The areas 1,2,3 corresponds respectively to the orthorhombic, amorphous and strained fractions. Rows 13,14 give the values of α_c , the figures in parenthesis are the fraction of the two non-orthorhombic components namely the network and amorphous ones respectively. The amorphous fraction is higher for the P-film whose crystals have grown faster than those of the S-film. The FTIR bands measure without ambiguity the orthorhombic organization, the sum of long- and short-range order in this crystalline modification as explained in the Appendix 2. The values of α_c FTIR are higher for the P- and S-films than α_c (X-rays) and α_c (DSC) due to the inclusion of short-range order not seen by X-ray spectra and not meltable in DSC. The sum of short-range and long-range orthorhombic order in the S-film (0.72–0.75) has the same value as the fraction of the less mobile phase as seen by ^{13}C NMR in the two-phase decomposition (0.71–0.75). In the S-films, the crystals have grown in equilibrium conditions, leaving only a small fraction (0.12) of strained phase and the same amount of amorphous phase (0.13–0.16).

From the results on the S-films one can write:

$$\begin{aligned} \alpha_c (\text{FTIR}) - \alpha_c (\text{X-ray}) \\ = \text{short-range orthorhombic order,} \end{aligned} \quad (3)$$

$$\alpha_c(\text{FTIR}) - \alpha_c(\text{DSC})$$

= orthorhombic order not meltable in the fast T - ramp

(4)

The short-range orthorhombic order from Eq. (3) is found somewhat larger for the S-films (0.2) and smaller for the P-films (0.13–0.16). The rapid crystallization of the P-films leads to a small amount of the short-range orthorhombic order which is nevertheless higher for the ZN (0.16) than for MT (0.13). Although the difference is not large, this is due to the faster kinetics of crystallization of the linear fraction of chains present in ZN. Using the combined X-ray and FTIR analysis, LLDPE samples can even include four fractions since the long- and short-range orthorhombic order can be separated by Eq. (3).

Several papers have investigated the possibility of inclusion of the butyl side chains in the orthorhombic phase. When the orthorhombic phase is analyzed as long-range order by X-rays, the chains with butyl groups are found excluded from the orthorhombic cell. The analysis of the relaxation behaviour of the –CH– groups at the branching point leads to the conclusion [2] that the butyl branches are equally distributed in the rubbery/amorphous and interfacial/network fractions in samples crystallized from the melt. In the fraction of short-range orthorhombic order defined by Eq. (3), the butyl groups are present but they do not prevent the chains to be organized in a cell which is part of small crystals but is still an orthorhombic cell. The values of α_c (FTIR) for the nascent samples are not reported here. The CH₂ rocking region of Fig. 3 below shows the large fraction of strained bands present in the nascent samples.

The non-orthorhombic phases: In the S-films, the strained fraction is small and identical (0.12) for MT and ZN, a result consistent with the slow growth of crystals in solution which leads to a reduced strain in the crystals. It is the amorphous phase (0.13 and 0.16) which reflects the small difference of crystallinity of the ZN and MT films. In the P-films on the other hand, the strained fraction is significantly higher in MT (0.20 instead of 0.14). The slower crystallization rate of the MT, in the conditions of formation of the P-films, increases the strained fraction and not the amorphous one.

Fraction with a high mobility: In the two phase model, $(1-\alpha_c)$ is the fraction with a high mobility in the sample which amounts to 0.4 to 0.6. This fraction of amorphous phase seems high and not too consistent with the cohesion of the materials and their melting points. On the other hand, the mobile fraction is found to be only 0.13–0.28 from FTIR and 0.35–0.36 by NMR (two-phase decomposition). These two techniques, by isolating an interfacial or network fraction where some order exists, give a description

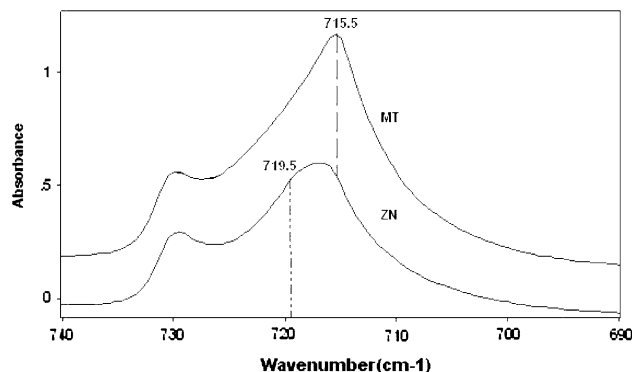


Fig. 3 Infra-red spectra in the rocking region of MT and ZN as nascent. The strained bands at 715–716 cm⁻¹ are seen without the decomposition necessary in Figs. 1–2. The band at 719.7 cm⁻¹ of the orthorhombic doublet has been partially overlapped by the strained band. MT appears to have a higher fraction of the strained band but band area values obtained through decomposition in the wagging region should confirm this

of the samples more consistent with their properties. The three phase decomposition in ¹³C NMR leads to a fraction of the mobile phase equal to 0.10 [2].

In resumé, Table 2 illustrates the fact that different techniques measure different order or restricted chain mobility at RT in the sample. The analysis does not reveal significant differences between MT and ZN, particularly for the S-films. The larger difference between the two samples is observed in condition of crystallization under moderate strain in the P-films. The network fraction is somewhat higher (by 0.06) for MT than for ZN. These two results indicate that differences have to be sought in samples submitted to strain, not in samples crystallized in equilibrium. The FTIR spectra permit to measure the short-range orthorhombic order not accessible by other techniques.

Part (II). Analysis of traces in a slow *T*-ramp

Table of ΔH_{ortho} and $\Delta H_{network}$

Events in the melt have been observed on a variety of polyolefins, homo- and copolymers. The range of temperature of evolution of the high-*T* endotherm is in the following order: linear PE < branched PE < copolymer. In a random PP-PE copolymer with stereoregular PP sequences and a small fraction of ethylene (0.03 for instance), the high-*T* endotherm is 30–40 K higher than that for the homopolymer [16]. This property can be compared to strain-hardening at high deformation found greater in copolymers than in homopolymers, Table 3 gives the characteristics of the melting traces of the nascent samples in different conditions. Rows 1,3 are for $\nu = 0.02$ K/min

Table 3 Characteristics of melting of nascent MT and ZN samples at slow, medium and rapid rate of heating

v^a K/min	Substrate	MT			ZN		
		T_m/T_c °C	ΔH_{ortho}^b J/g	$\Delta H_{network}^c$ J/g	T_m/T_c °C	ΔH_{ortho}^b J/g	$\Delta H_{network}^c$ J/g
0.02	Hg	118	130	130	126	95	137
0.1 ^d	Hg	111	−90	−112 ^d	119	−78	−82 ^d
0.02	Steel powder	122	93	250	126	99	233
0.2 ^e	Hg	118	135	83	126	133	64
10 ^f	Al	114	97	75	124–125	107	48

^a Data with a C80 Setaram calorimeter except those at 10 K/min (standard DSC)

^b Integration between 35 °C and 132 °C on heating and 87–123 °C on cooling

^c Integration between 220 °C and 270 °C (MT), 200–270 °C (ZN). For UHMW PE, integration on heating was 140–170 °C

^d Cooling trace. Integration of the high- T exotherm between 125 °C and 248 °C for MT and ZN

^e The cooling trace at the same v shows also a high- T exotherm

^f Without the slow calorimetry data, $\Delta H_{network}$, at that rate of heating, would not have been recognized

for two substrates, Hg and stainless steel. Rows 4–5 give, for comparison, the characteristics of the traces at two higher v , namely at an intermediate value 0.2 K/min (on Hg) and at the usual rate of 10 K/min (in aluminium standard cells). Row 2 is for the crystallization trace. Columns 3–5 give the values of T_m/T_c , ΔH_{ortho} and $\Delta H_{network}$ for MT and columns 6–8 the same data for ZN. When v is low, (rows 1–4), $m = 32$ mg while it is 3–4 mg for $v = 10$ K/min (row 5). Data in the table are obtained by averaging over the number of runs made (3–4, for the slow ramps). The interval of T used for measuring $\Delta H_{network}$ is given in the footnotes of Table 3.

Analysis of traces with $v = 0.02$ K/min

Figures 2 and 4 give an example of the traces of melting on stainless steel for MT and ZN. Figure 5 represents the cumulative heat fraction of the endotherms versus T for (MT, ●) and (ZN, ■). The value of ΔH for each segment is divided by the total enthalpy of the trace so that the ordinate of Fig. 5 varies between 0 and 1.0. *Low- T region.* The difference in the T_m values which is 10 K in standard conditions has diminished to only 4 K due to the annealing of MT. The methyl-rich fraction of ZN is seen clearly to melt continuously from 65 °C on, while the initially less crystalline MT starts melting 30 K higher at 95 °C. The main peak of fusion is narrower for ZN, observed also in standard conditions. Small exothermic and endothermic events are more prevalent in MT. It is to be noted that, in spite of the very slow ramp, the endotherms of melting have the same characteristics (shape and width) as those a rapid ramp. This is due to the large sample mass used in the experiment which reduces heat transfer and prevents the deformation of the orthorhombic crystals which would take place with a slow ramp and $m = 2$ –3 mg.

Medium- T region. Between 135 °C and 180 °C, the two melts are different: the melt of ZN shows a continuous exotherm (apart for a short endothermic spike at 160 °C) while between 135 °C and 180 °C, two endotherms and two exotherms are observed for MT.

High- T region. The main features are the following: (i) On Hg, a conductive substrate which nevertheless cannot be mixed with the small beads of the nascent material, the high- T endotherms have the same magnitude as that of the main endotherm (Table 3). The end of the endotherm which was at a lower T (about 160–170 °C) for a nascent high density PE [5] is now around 270 °C. (ii) The stainless steel substrate has the effect of increasing $\Delta H_{network}$ to the extent that $\Delta H_{network}/\Delta H_{ortho}$ is now ≈ 2.4 . ΔH_{ortho} is unchanged or reduced, an effect found on iPP [7]. (iii) The traces reveal a difference between the two samples concerning two points namely the range of T on which $\Delta H_{network}$ evolves and the irregularities of the trace. The endotherm ranges continuously over 90 K for ZN (180–270 °C) with a maximum at 215 °C. The endotherm evolves over 60 K for MT (210–270 °C) with two maxima at 230 °C and 260 °C. These features are common to different runs on the same substrates and to the Hg and stainless steel substrates. They will be commented upon following the proposed molecular origin of the endotherms.

Second run

The second run of a sample have been done after slow calorimetry after crystallization in different conditions. Traces were taken by slow calorimetry and DSC. As said in the experimental part, the main melting endotherm which reveals the orthorhombic crystals present in the solid is not changed by events in the melt. The growth of orthorhombic crystals is thermodynamically so favourable that the state

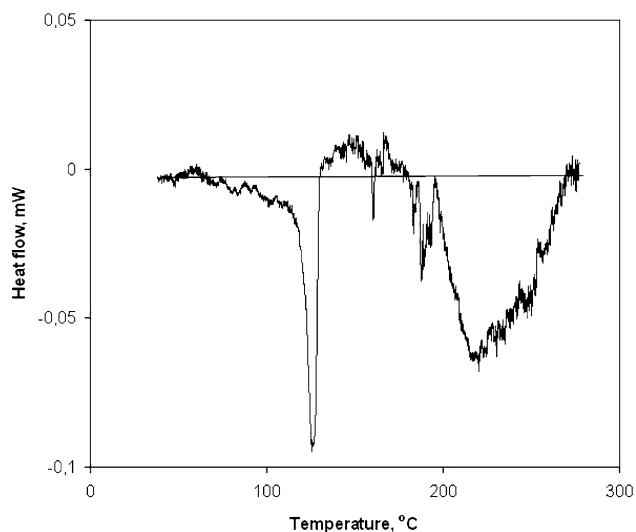


Fig. 4 Slow calorimetry trace of ZN on a stainless steel substrate. $v = 0.02$ K/min. $m = 30.9$ mg. Weight ratio, substrate/sample ≈ 100

of the melt does not affect this growth. When the second run is made with a slow ramp, $\Delta H_{\text{network}}$ is smaller than in the first second run, a difference with the linear (UHMWPE) [5] where it was significantly higher. The reason for this difference is not clear except the much higher temperature for the evolution of $\Delta H_{\text{network}}$ for LLDPE's.

Part III Molecular Origin of the high- T endotherms and support for it

The interpretation of the events in the melt should be consistent with the following findings

- i. The magnitude of the events and the temperature at which they take place depend on catalyts used for

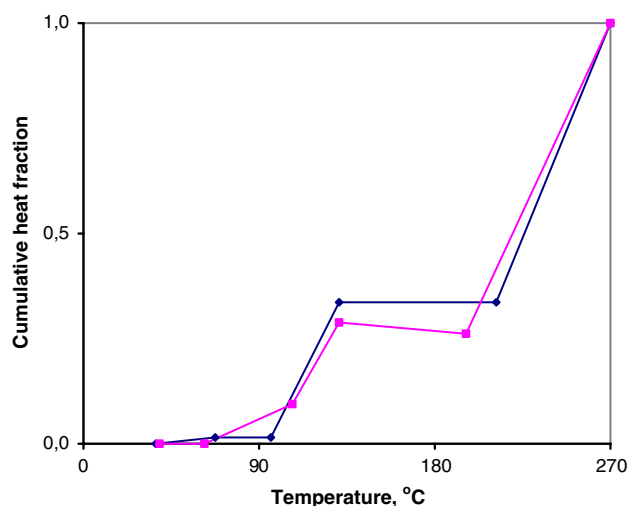


Fig. 5 Cumulative curve of the traces of Figs. 2, 4. $\Delta H(T)/\Delta H_{\text{total}}$ is plotted versus T . The events occur at higher temperature for MT

synthesis and on the history of the sample (Figs. 2, 4, 6).

- ii. High- T endotherms are also observed ($\Delta H_{\text{network}}$ (on Hg) ≈ 60 – 100 J/g) in samples with few entanglements such as low MW linear standard PE samples [36] used for characterizing MW distribution [31].
- iii. In some conditions, exotherms usually with a fast kinetics [6, 30] are found on the low- T part of the melting traces.
- iv. The high- T endotherms can overlap the melting of the main crystals and be larger than $\Delta H_{\text{melting}}$ of perfect crystals. This happens when the heat conductivity is increased [7, 30] and/or when a sample already deformed mechanically by extrusion is melted in non-standard conditions in a DSC [30].
- v. The kinetics of these events are slow, not to be compared to the melting/crystallization of long-range order.
- vi. The events are reversible as indicated on Table 3, exotherms being seen on cooling slowly [4–10]. The fact that, in some conditions, $\Delta H_{\text{network}}$ evolves in the high- T part of *cooling* ramp [30] suggests that the residence time as much as the temperature leads to the events.

The features described above (high value of $\Delta H_{\text{network}}$, events in low MW samples, displacement of the endotherms, traces of deformed samples) and the reading of an article on PS melts [25], suggested by a reviewer, lead the authors to revise the origin of $\Delta H_{\text{network}}$. The initial findings, their interpretation and the consistency of the new model with the early calorimetric work are presented in Appendix 1.

In ref [25], the flow of PS at 170 °C has been investigated by several techniques such as neutron scattering, flow

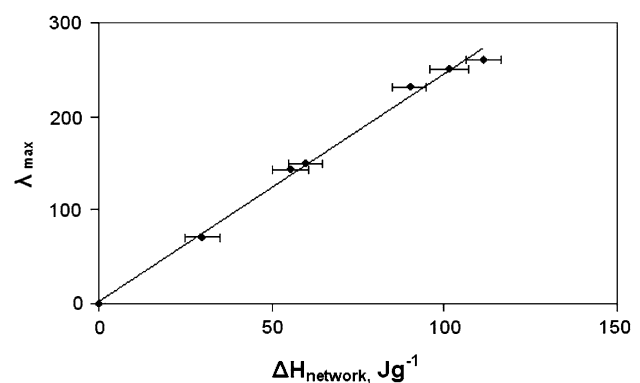


Fig. 6 Films of UHMW PE prepared from semi-concentrated solutions in five different solvents. Correlation between their maximum drawability at 110 °C, λ_{max} and $\Delta H_{\text{network}}$ from the slow calorimetry traces. With permission of the Journal of Materials Science [11]

visualization and molecular theory. The macroscopic and microscopic configurations of the entangled molecules were followed. Fundamental processes take place in the movement of the long-chain molecules namely reptation, contour length fluctuation and release of constraint. One of the conclusions of the investigation was that “orientation at the length scale of the entire chain decays considerably more slowly than at the smaller entanglement length”. The conditions of heat conduction and flow in the PS experiments ($m = 500$ mg, $T = 170$ °C) are somewhat different from those in slow calorimetry ($m = 32$ mg, $T = 150$ – 250 °C). Nevertheless, predicting a comparable behaviour in the orientation decay of PE and PS chains is reasonable: the endotherms observed in Figs. 2, 4 and 7b are associated with the slow decay of chain orientation. This is the second step of cooperative motions during the ramp, the first being the chain orientation itself. The exothermic effect of chain orientation overlaps with that of the endotherm of melting of the orthorhombic crystals but is observed in some

conditions. When the decay is not observed, the reason is that orientation has not proceeded due to a too fast ramp or because the sample was too crosslinked to be deformed. An example of the memory of the melt comes to mind: The dissolution of beads of nascent P4MP1 ($T_m = 240$ °C) placed with nC7 ($c = 10\%$) in a sealed flat cell was observed under the microscope in a slow T -ramp up to $T_d + 20$ K. The beads, the contour of which had disappeared at T_d were seen again on cooling slowly as if the chains had not moved in the solvent.

The following results on gels, on a standard low MW sample and on calorimetric and IR data as a function of T are presented because they support the model:

Relation between $\Delta H_{network}$ and mechanical properties (λ_{max})

Sample deformation during drawing at about $T_m - 20$ K and extent of melt deformation in a slow T -ramp must relate to similar characteristics of the materials. It is then worthwhile to recall previous results involving drawability and slow calorimetry [11]. Films of UHMWPE obtained from gels prepared in different conditions (solvent, concentration, stirring) were submitted to a slow T -ramp and to drawing. Figure 5 shows the correlation between λ_{max} the maximum drawability, at 110 °C, and $\Delta H_{network}$ of the same material in the T -ramp. Finding the conditions to reach a high drawability for a film is an art because this property is the result of a balance of different morphological features of the material [37].

Partial disentanglement and stable orientation of the chains take place during the vigorous stirring used for obtaining an homogeneous solution. When the films dries the pre-oriented fraction stays as such. During drawing on one hand and slow calorimeter ramp in the calorimeter on the other hand, chains continue to stretch and to align without rupture. This transformation is followed by the measurement of λ_{max} in the drawing experiment and usually not seen very well in calorimetry due to overlapping with $\Delta H_{melting}$. Slow calorimetry is able to measure, through $\Delta H_{network}$, what comes later in time and temperature, namely the decay of the orientation.

Slow calorimetry of a low MW standard

FTIR and calorimetric analyses ($v = 3$ K/h) of a linear standard, $M_w = 13,600$ and $M_w/M_n = 1.1$ have been done. The FTIR analysis of the rocking region gives as expected, $\alpha_c = 0.85$ and a small amount of the non-crystalline phases (0.07, 0.08). The high- T calorimetric event is made of two endotherms, one around 200 °C (1) (≈ 48 J/g) and the other around 250 °C (2) (≈ 64 J/g). This pattern is quite frequent in non-standard samples. The signal between (1) and (2)

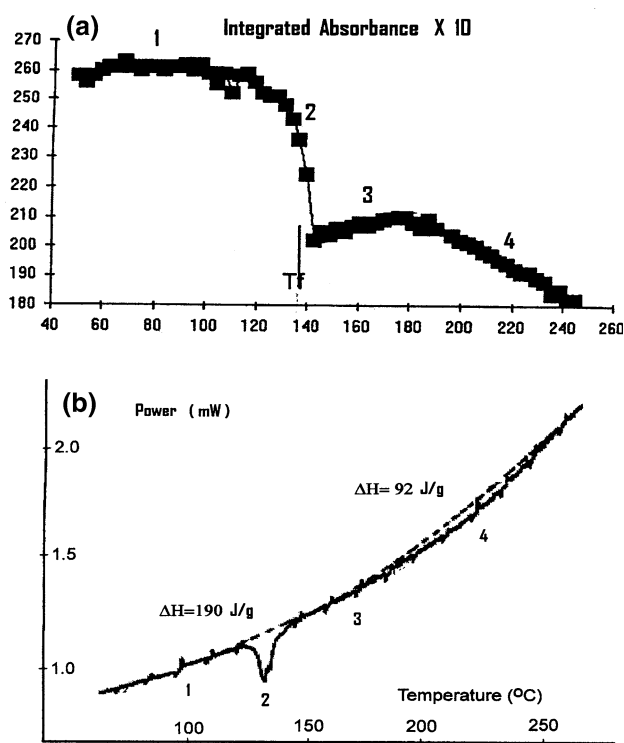


Fig. 7 Integrated absorbance Abs(T) in the rocking region and calorimetric trace between 50 °C and 250 °C for a low MW linear sample. (a) Abs(T) shows four different regions : 1–2 before and during melting, 3–4 in the melt. The sharp drop of Abs(T) in 2 is due to a change of sample density at T_m . The increase in Abs(T) in 3 is associated with ordering/densification and the decrease in 4 to relaxation of chains and expansion. (b) Slow calorimetry trace showing four different regions: 1–2 before and during melting, 3–4 in the melt. Note that athermal effect in 3 coincides with the densification in (a) and the endotherm of $\Delta H_{network}$ in 4 starts at the same temperature as the drop in Abs (T) in a

which shows a region of athermal or slightly exothermic events may be a tracer of the orientation which takes place between the two regions of orientation decay.

Comparison of FTIR in the melt and slow calorimetry between 50 °C and 240 °C for a low MW sample

Orientation before decay can apparently be seen un-expectedly in FTIR experiment. The FTIR analysis in the melt was not made for ZN and MT but for a linear PE of low MW whose characteristics are $M_w = 35,000$, $M_w/M_n \approx 3$, $MI = 37$, α_c (FTIR) = 0.85, $\alpha_{\text{amorphous}}$ (FTIR) = α_{network} (FTIR) = 0.07–0.08.

In Fig. 7a, b, the integrated absorbance of the rocking regions and the calorimetric trace are plotted against T between 50 °C and 250 °C with $\nu = 0.05$ K/min. The value of ΔH_{ortho} (190 J/g) is as expected for a linear sample. $\Delta H_{\text{network}}$ (92 J/g) is in the range of values found on Hg as substrate and this rate of heating. Four regions appear in the Fig. 7a (as in Fig. 7b). In (1), below T_m the absorbance of the rocking region is quite independent of temperature. The variation of the absorbance is less than 3%. As said in the experimental part, FTIR data are quantitative. The drop of absorbance in (2) is due to melting. The decrease of the absorbance is 20% and equal to the well-known change of density for PE at melting. As the beam goes across less packed chains, the integrated absorbance is smaller. In (3) the absorbance takes an unexpected trend since it increases steadily up to 180 °C while it should continue to diminish due to the expansion of the chains. This is interpreted as showing the process of orientation between the chains leading to densification of the material. The decrease of the integrated absorbance in the (4) region coincides on Fig. 7b with the start of the endotherm. In the present conditions, one cannot distinguish in the signal the part due to the decay of orientation from that due to normal expansion of the melt. The same IR measurement with a rapid T -ramp where there is enough time for expansion but not enough for decay could be done to clarify this point. The thinness of the films in these measurements (50–70 μ) is an advantage to see events in the melt since the sample thermal conductivity is higher than in a thick film.

The preparation of high modulus fibers by drawing is made with gels of linear PE, which probably are more easily drawable than the branched samples. Interpretation of the difference between MT and ZN in the high- T region of the traces of Figs. 2, 4 is possible knowing their respective composition. The linear fraction of ZN orients and decays at somewhat lower T than its branched fraction. The MT trace displays a continuous endotherm between 210 °C and 270 °C and a maximum displaced compared to that of the ZN trace. On the cumulative curve, Fig. 4, the

fraction of $\Delta H_{\text{network}}$ which has evolved at 215 °C is 0 for MT (point at the end of the horizontal line) and 0.17 for ZN. The data are slightly different in Table 3 and Fig. 4 because of the averages and also because the small endotherms and exotherms are not counted in the integration for the data in the table but they are in Fig. 4.

Reversibility of events in the melt: Row 2 of Table 3 gives the characteristics of the cooling traces at 0.1 K/min. Exotherms evolve between 250 °C and 126 °C ending a few K before T_c . The exotherms are flat but with a maximum signal at around 180 °C for MT and 10–15 K lower for ZN. The range of temperature of the exotherms indicates an early reordering in the melt, accompanied by fractionation according to composition and MW in the heating ramp. Ordering of the melt in the first ramp in presence of nucleus of crystallization and tight entanglements has a different kinetics than that which occurs after the slow ramp [36]. Another expression of this order would be to invoke the existence in some conditions of the melt of a pseudohexagonal phase whose not very clear X-ray pattern has been reported.

Part (IV) FTIR analyses of samples after different histories: nascent and thermally treated

Difference between ZN and MT by FTIR at RT

While the rocking regions of S- and P-films were analyzed above for α_c determination, the nascent samples are now reported as well as the wagging, bending and stretching regions. The sensitivity to crystallinity, orientation of lamellae and strain of the different regions i.e., of the different movements of the atoms in the CH_2 groups or of the chains has been investigated mainly in the rocking region because with standard film preparation, the other bands (except the wagging) are saturated for $e > 20$ –40 μ .

Rocking region of the nascent samples: Figure 8 shows the rocking region of the nascent samples. One notes two main differences with Figs. 1a, b, where the crystals have little strain, regarding the position of the bands and the absorbance. The strained bands at 715–716 cm^{-1} are observable without the decomposition which was necessary to detect them in the S- and P-films. Also, the absorbance is lower and the band-width larger. MT has a higher fraction of the strained band than ZN. This was noted on several different runs of the beads but because of the variability of the spectra of the nascent samples, one should analyze quite a few of them to ascertain the difference between the two samples.

Wagging region for S-, P-films and nascent.: This region has the CH_3 umbrella mode of branch end groups at 1378 cm^{-1} and the gauche region (bands at 1,368, 1,350, 1,320 cm^{-1}). Figure 8a–c show the wagging region for S-, P- and nascent films of different e . For the three histories,

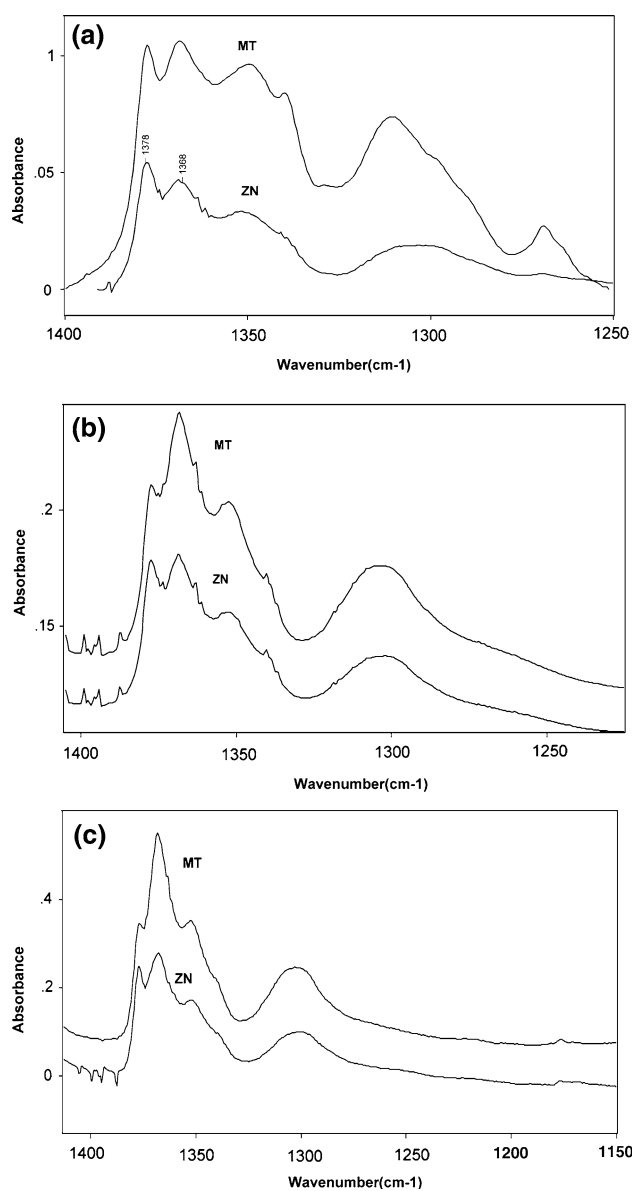


Fig. 8 The wagging region (a), (b) and (c) are respectively for S- and P-films and the nascent. For the three histories, the absorbance at 1368 cm^{-1} is larger for MT than for ZN

the maximum absorbance of the $1,368\text{ cm}^{-1}$ band is higher for MT even if the values of α_c (MT) and α_c (ZN) are little different (last two lines of Table 2).

Decomposition of the wagging region: Figure 9 is an example of decomposition of nascent MT with six bands between $1,200\text{ cm}^{-1}$ and $1,400\text{ cm}^{-1}$. Table 4 gives the fraction of each band obtained by Eq. (1). The fractions of the $1,368\text{ cm}^{-1}$ band are very similar (0.269 and 0.260). The higher maximum absorbance reported in Fig. 8a–c gives a valuable molecular information on MT namely that the environment of this vibration is in a more homogeneous in MT than in ZN, a reflection of the regular distribution of methyl groups along the MT chains. The integrated

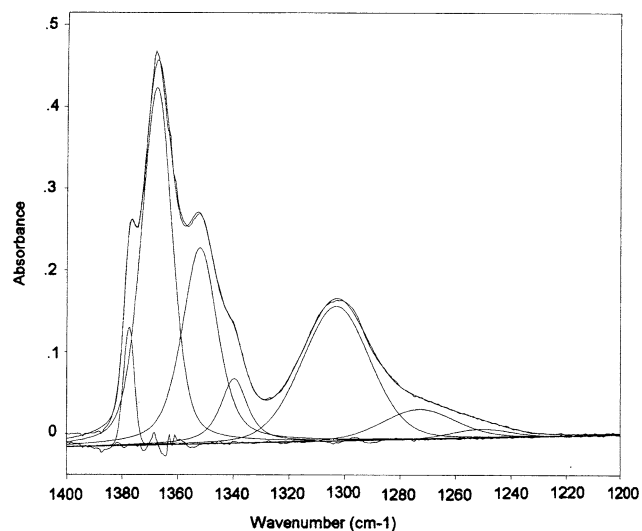


Fig. 9 Example of decomposition in the wagging region for the nascent sample. The fractions of the $1,368\text{ cm}^{-1}$ band, are similar (0.260 for MT and 0.269 for ZN)(Table 4). The higher maximum absorbances for MT, seen in Fig. 8, indicate that the band is narrower for MT than for ZN, due to a more homogeneous environment

absorbance complements the description of the sample given by the maximum absorbance. The concentration of folds is higher for MT, which does not contain long linear segments in the chain. The higher absorbance at 1302.8 cm^{-1} (0.317 compared to 0.267) is related to the lamellar thickness found smaller for MT [2].

The CH_2 stretching region of thin films

In the crystalline regions, the bands are narrow due to the homogeneity of the environment. As a consequence, the maximum absorbance, is higher than in the amorphous regions. The integrated absorbance, and the extinction coefficient, ϵ , do not have to be higher. For the rocking regions, as said in the experimental part, the extinction coefficient is not very different for the large bands of the amorphous and strained regions and the orthorhombic doublet. On the other hand, the CH_2 stretching region ($2,700\text{--}3,100\text{ cm}^{-1}$) seems to vary greatly with the sample history as will be shown below. To follow quantitatively the change in ϵ (CH_2 stretching) with treatment, very thin films have been prepared. The spectrum of a S-film with $e = 12\text{--}15\ \mu$, between 600 cm^{-1} and $3,500\text{ cm}^{-1}$, is shown in Fig. 10a. The maxima of the CH_2 stretching bands at 2849.2 cm^{-1} and 2918.1 cm^{-1} are about eight times that of the rocking. In Fig. 10b, the spectrum of a treated film, with $e \approx 30\ \mu$, after slow heating and slow crystallization illustrates the change. The maxima of the CH_2 stretching bands are now only about twice that of the rocking. The small bands of the wagging increase as well as the doublet at

Table 4 Decomposition of the gauche region of the MT and ZN nascent samples

	Peak position λ (cm ⁻¹)	1377.9	1368.4 ^a	1352.9	1340.0	1302.8 ^b	1258.4
MT ^{c,d}	Fraction	0.076	0.260	0.207	0.074	0.317	0.066
ZN ^{c,e}	Fraction	0.160	0.269	0.200	0.090	0.267	0.016

^a The integrated absorbances are similar for the two samples while the maximum absorbance is higher for the MT samples (Fig. 9)

^b This band, associated to the GTG and GTG' conformation, is larger for the MT samples

^c Samples with medium strain in the rocking have been chosen for the decomposition. Average of the spectra of two runs

^d Area_{rocking} = 19.4; Area_{gauche} = 10.1

^e Area_{rocking} = 13.9; Area_{gauche} = 7.4

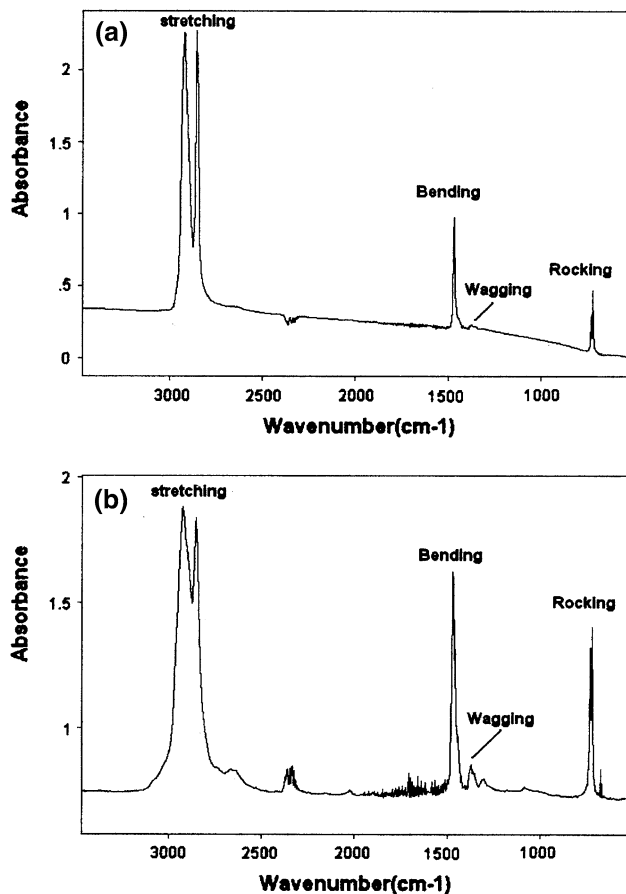


Fig. 10 The PE spectra of thin films with the CH₂ rocking, CH₂ bending, CH₂ wagging and CH₂ stretching regions. (a) A S- or P-film prepared in standard conditions. (b) A treated film (heating at 0.2 K/min and cooling at 0.1 K/min). With a slower rate and slower rate of cooling (0.05 to 0.016 K/min), the maximum absorbance of the stretching peaks is reduced progressively to half of that of the rocking

2,630–2,660 cm⁻¹. After a slower crystallization, the ratio of the maximum absorbance of these two regions falls from 2 to 0.5.

In Table 5, values of areas of the rocking and stretching regions are listed with ε (CH₂ stretching) for the S- and P-films and for treated films. The first and second rows are for cooling in standard conditions. The high value of ε (CH₂

stretching) in the second row comes from the spectra of ultra thin films made from a highly disentangled solution and a relatively fast evaporation. The third row of Table 5 gives the range of ε (CH₂ stretching) for MT and ZN cooled at $v_c = 0.1$ K/min. When $v_c = 0.0167$ K/min, ε (CH₂ stretching) falls from 3.7 to 5.3 to ≈ 1 . The films are less transparent with a base line absorbance of 1–1.5 instead of the usual 0.2–0.3. The shape of the bands is greatly changed, the two bands of Fig. 10a, b being replaced by a flat plateau. One sees the early beginning of this shape in Fig. 11b below. Spectra of PE fibers (DMS company and this lab) have been taken for comparison. The rocking bands has the usual profile with a rather low crystallinity but the stretching region has the characteristic plateau shape. The fourth row is for dried gels made from semi-concentrated solutions. The value of ε (CH₂ stretching) is large again with broad bands. The rocking region on the other hand is changed by the treatment but not dramatically: The ratio of the 719.4/730.5 is higher than in the

Table 5 Extinction coefficients, ε , of the CH₂ stretching band as function of sample history

Sample	Area (CH ₂ rocking) ^b	Area (CH ₂ stretching)	ε CH ₂ stretching ^c	n^d
S- P- films ^a	2–10	70–350	12	10
S-films ^e	2–3	105–160	18	2
Slow heating/slow cooling ^{f,g}	10–30	170–400	3.7–5.3	12
Slow heating/quenching ^h	20–30	— ⁱ	20–30	4

^a Standard Preparation

^b With ε (rocking) = 0.34, the value of ε for treated films is calculated when measurement is difficult

^c $\varepsilon = \text{Area}_{\text{stretching}}/e$

^d Number of runs

^e From highly disentangled solutions

^f T -ramps: 0.02 K/min (heating) and 0.1 K/min (cooling)

^g When the T -ramp on cooling is 0.0166 K/min, ε (CH₂ stretching) ≈ 1

^h S-film from a 10% solution

ⁱ Very wide bands with absorbance near saturation

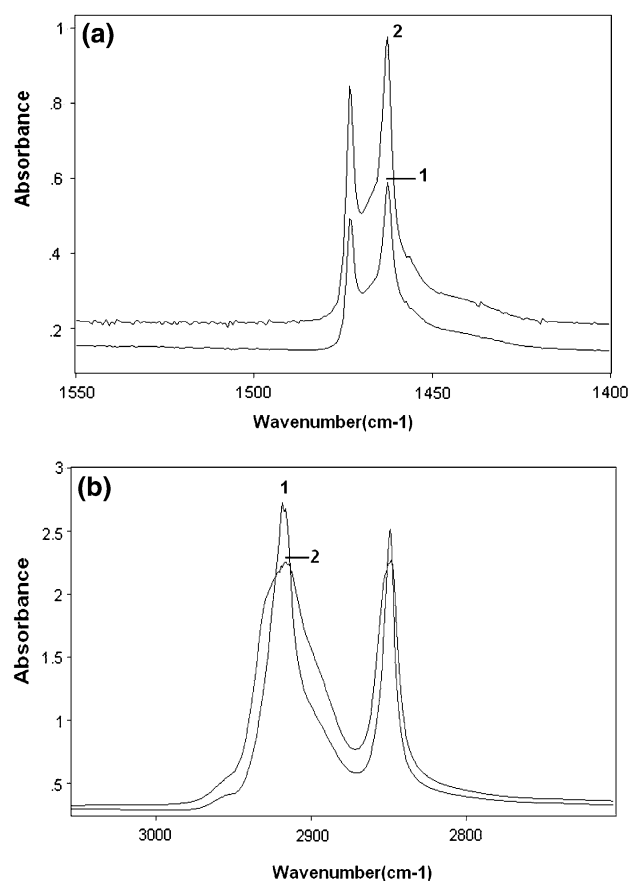


Fig. 11 Sensitivity of the CH₂ stretching region of very thin not treated S-films to the sample history (Table 5 for ϵ values). **(a)** Spectra in the CH₂ bending region for ZN (1) and MT(2). The S-film of MT is thicker and was crystallized somewhat faster than ZN. The bands have similar shape with the areas S such as Area(MT)/Area(ZN) = 1.45. The bands in the rocking region (not shown here) are also very similar and their areas in the same ratio. **(b)** Spectra in the CH₂ stretching region for ZN (1) and MT(2). The two symmetric CH₂ stretching bands at 2,849 cm⁻¹ have the same shape but the absorbances are not in the ratio of the rocking and bending regions. The antisymmetric stretching at 2,918 cm⁻¹ has two clear shoulders. Area(MT)/Area(ZN) = 1.3. The values of ϵ (CH₂ stretching) are now 16 for MT and 18 for ZN. This spectrum is shown because it displays an intermediary shape of the bands not visible in the bending and rocking regions. After a slower cooling, the two bands overlap and form a large plateau

equilibrium films and α_c (FTIR) = is low (0.5). Our interpretation of these effects on ϵ (CH₂ stretching) is as follows:

The crystallization, in the solvent and under the press of the S- and P-films, induces a special stacking of the lamellae, which creates a homogeneous environment of the vibrating CH₂ groups and narrower bands. High values of α_c (FTIR) and few gauche conformations are a result of the quasi-universal mode of film preparation. Slow crystallization from the melt is a standard strategy for obtaining a high value of α_c at RT. Usually crystallization is isothermal near T_c found in a T -ramp, followed by aging. The

characteristics of the sample after a slow T -ramp are not as paradoxical as appears. The chains between 250 °C and 150 °C, for instance, have every chance to reach an equilibrium state which is different from that which exists at the much lower T_c . The arrangement of crystals which does not change the crystallization/melting traces at T_c or T_m in the rerun, is nevertheless different. One can speculate that it contains many nuclei which favours at T_c the growth of many small crystals oriented at all angles from the surface, the chains having many conformations. The CH₂ stretching vibrations are in an environment not too unlike that from the melt where the two peaks are replaced by a broad band. The lens-like appearance of the material is the macroscopic effect of the arrangement. The value of T_c at the end of a slow ramp is higher than in a rapid ramp but it was attributed only to a kinetics effect. The spectroscopic description is that the average moment of the incident light and of all CH₂ stretching vectors has changed and in consequence the absorbance. Calorimetry at the second melting has not the sensitivity of the IR bands and recognizes only a lower ΔH_m .

The greater sensibility of the CH₂ stretching region to the chain arrangement is illustrated by the spectra of two thin films whose bending and stretching regions are displayed in Fig. 11a, b. In the bending region, (Fig. 11a), the ratio of the two integrated absorbances (Area(MT)/Area(ZN) = 1.50) reflects their difference in e . The spectra are not homothetic since the ratio (MT/ZN) of the maximum absorbance at 1462 cm⁻¹ is 1.7, higher than expected from their relative thickness but the profiles of the bands are similar. The trend of narrower bands for MT is the same as in Fig. 8. The band widths at mid-height are slightly different 12.7 cm⁻¹ for MT and 13.0 for ZN. In the CH₂ stretching region (Fig. 11b), the ratio of the integrated absorbance between 2,600 cm⁻¹ and 3300 cm⁻¹ Area (MT)/Area (ZN) is 1.26 while that of the maximum absorbance is 0.87. In the CH₂ stretching region, MT and ZN have a different range of conformations, hardly noticeable in the bending bands. Furthermore, the bands in MT starts to be multiple. Two shoulders appear at \approx 2,950 cm⁻¹ and 2,890 cm⁻¹ on both sides of the antisymmetric band. When many more different conformations will be present, the two bands corresponding to the symmetric and anti symmetric stretching, will be transformed into a flat plateau probably for both samples but the change will start for MT with a milder treatment.

This higher sensitivity of a thin MT film to deformation is believed to be relevant to the present question of the difference in processing of MT and ZN. The analysis of the CH₂ stretching region, not found in the literature for films which are not nano-films, has a potential for giving new information on treated or deformed samples.

Conclusion

The objective of the present work was to find differences between two LLDPE samples synthesized with Metallocene (MT) and Ziegler Natta (ZN) catalysts. Several standard techniques (X-ray, DSC, FTIR spectroscopy) and a non-standard one, namely slow calorimetry, were used. This paper presents new results and interpretations in slow calorimetry and FTIR.

The MT and ZN films prepared in standard, equilibrium, conditions do not reveal significant differences of crystallinity. The high temperature endotherms ($\Delta H_{\text{network}}$) found in the melt by slow calorimetry ($\nu = 0.02$ K/min) evolve at higher temperature for MT. In previous work, $\Delta H_{\text{network}}$ was associated with the slow melting of strained order in a physical network. However, reading about chain motion in PS chains at high T [25] and recent results in non-standard calorimetry [30] convinced the authors that other effects with a larger potential of absorbing heat, are also at work. The slow T -ramp undoubtedly orient the chains which, after enough time at high temperature, loose their orientation. The $\Delta H_{\text{network}}$ is associated now with the slow decay of orientation. The difference in the calorimetric traces of MT and ZN is attributed to a sizeable fraction of linear chains in ZN. Slow calorimetry of linear samples at the same ν suggests that chains without side groups lend themselves more easily to orientation/disorientation and consequently to a lower T for $\Delta H_{\text{network}}$. The high- T exotherms observed on cooling (248–125 °C) indicates a early reordering in the melt, facilitated by the fractionation according to composition and MW taking place during the heating ramp. The relationship between the maximum drawability, λ_{max} , and $\Delta H_{\text{network}}$ for films with different histories can be understood after recognizing that drawing a gel using a mechanical device or using the T -ramp of the calorimeter corresponds to comparable molecular processes.

The integrated IR absorbance of the rocking region, $\text{Abs}(T)$, is measured between 40 C and 240 C and compared with the slow calorimetry trace for a low MW sample. A correspondence between two regions in the melt can be made with the two techniques. The presence, above T_m , of a domain of temperature (142–180 C) where densification and chain ordering take place before the slow orientation decay (180–245 C) supports the origin of $\Delta H_{\text{network}}$ presented in this paper.

The materials after a slow melting are analyzed by standard DSC and FTIR to evaluate the effect of the high- T treatment on the crystallization process. When the slow ramp is followed by fast cooling, the melting characteristics are standard. However, slowly crystallized samples have a lens-like appearance and different spectra. The new finding in FTIR is about the little-studied CH_2 stretching region. In very thin films prepared in standard conditions,

the extinction coefficient, ε (CH_2 stretching) is measurable and equal to 12. It decreases to 3–5 with $\nu_c = 0.1$ K/min and even to 1 for $\nu_c = 0.0167$ K/min. This is interpreted as showing that materials so grown have small crystals, oriented in every direction inside the lens, and a high proportion of tie chains and gauche conformations. Due to their special sensitivity to changes of conformations, the CH_2 stretching bands have the ability to reveal in thin films, thermally treated or not, different histories not noticeable in the rocking or bending regions. Information on the sample morphology after a slow thermal treatment should be completed by other techniques.

The events on the calorimetric traces of MT and ZN, are seen as tracers of happenings in melts during processing. Difficulties in extruding MT, such as irregular flow and fluctuation in viscosity, can have a common origin with the succession of exotherms and endotherms of its trace. The presence of a fraction of linear chains in ZN facilitates a smoother alignment and expansion of the branched fraction in the T -ramp. Raising the extruder temperature for the MT polymers could improve processing.

Acknowledgements The authors acknowledge the financial support of the NSERC (General grant) and also of a support from Estac (Environmental Science and Technology Agency of Canada). The Bayer company (Sarnia, Ont.) who supported the Estac project gave graciously the samples of LLDPE.

Appendix 1: Analysis by slow calorimetry

Our investigation of polymers melting using slow calorimetry has its origin in the study of UHMWPE gels [6]. The heat of dissolution, ΔH_{diss} , at $\nu = 0.0167$ K/min measured by integration up to the end of the main peak was found to vary with the solvent. It was for instance 265 J/g in trichlorobenzene (TCB) and 200 J/g in decalin. Melting without solvent in the same conditions gave $\Delta H_{\text{melting}} = 200$ J/g. When the T -ramp was continued above T_m/T_d , a high- T endotherm, $\Delta H_{\text{network}}$, was revealed which added a complement to the main peak. Our interpretation was the following: the entangled/network fraction of the material contains some short-range order, the melting/dissolution of which is displaced at higher T because of the strain generated by the T -ramp itself. Strain, as does pressure, shifts T_m towards higher temperatures or renders the order unmeltable in the conditions of the experiment. A slow T -ramp leaves time for the chains to respond in an equilibrium situation to the inescapable expansion. The kinetics of melting/dissolution is slow because strain continues to grow in the ramp. In the linear sample, integration was not pursued above 170 °C. The effect of the solvent on ΔH_{diss} is interpreted partly in terms of thermodynamics [11]. Analysis of a variety of polyolefins [7–11] and of

amylose (mixed with water) [12, 13, 17] confirmed the generality of the effect of strain on dissolution and melting. This research led to the understanding of the effect of strain-building on phase-change or other properties [4] and explained ambiguous results reported in the literature.

The present modified model can explain also the events observed on UHMWPE which are seen to involve also two steps. The first step is chain extension (strain-growing) and the second orientation decay (disordering of short-range order). One difference between the two descriptions covers the two steps and is somewhat more than linguistic: chain extension englobes all the chains not only the entangled chains of the network. The other difference is that an exotherm accompanies dissolution and melting and a tracer of chain extension. It has been observed as a sharp peak on gels but not in solids. The exotherm of extension/orientation has a slow kinetics with an enthalpy which overlaps ΔH_{ortho} and ΔH_{diss} and reduces them. In a polydispersed sample, exotherms and endotherms are likely to overlap. Orientation during the ramp depends on the conditions such as solvent-dependant swelling for the dissolution ramp and on the branch content for the melting ramp. The advantage of decay of chain orientation over melting strained order is that its magnitude has no obvious limit so that it can cover the large values of $\Delta H_{\text{network}}$ found with MT and ZN and with DSC in non-standard conditions [30].

Appendix 2: IR spectra of PE

The assignment of trans- and gauche conformations in the methylene chain has permitted to identify the ordered and less ordered regions of PE. Most of the analyses rest on a two-phase description of a semi-crystalline polymer. However, other bands are seen in the spectra of films submitted to mechanical deformation, which have been assigned to specific bands to deformed crystals. In highly deformed crystals these bands are observed visually on the spectra (Fig. 4), in less deformed films they are seen as a shoulder or by decomposing the main peak (Fig. 1). Decomposition of the bands leads to a quantitative measurement of the orthorhombic, amorphous and strained fractions at RT. The strained fraction is associated with monoclinic crystals and the network phase. The monoclinic IR bands can be seen even when the size of the monoclinic crystals is too small to give the X-ray pattern characteristic of the monoclinic modification. For this reason this fraction has been called monoclinic-like.

The IR spectra of the chains ordered in the orthorhombic and monoclinic modifications present a useful difference: in the orthorhombic modification, a very characteristic doublet in the rocking and bending regions is observed while a singlet appears in the monoclinic modification.

The doublet is due to the interaction of the chain in the centre of the cell with those on the sides. This interaction leads to a feature called field-splitting, i.e., to the presence of two bands for the same vibration. This effect does not take place in the amorphous regions or in the monoclinic modification because the chains are further apart. On a series of spectra taken between RT and the melting point T_m , expansion of the chains leads to a gradual increase of the amorphous phase and 5–7 K below T_m the doublet disappears [15]. Thanks to field-splitting, the fraction of the orthorhombic modification is measurable without ambiguity in the $-\text{CH}_2-\text{CH}_2-$ bending or rocking regions of the PE spectra.

References

1. Kitamaru R, Horii F, Murayama K (1986) *Macromolecules* 19:636
2. Kuwabara K, Kaji H, Horii F, Bassett DC, Olley RH (1997) *Macromolecules* 30:7516
3. Matter R, Stille W, Strobl G (1993) *J Polym Sci Polym Phys Ed* 31:99
4. Delmas G (1993) *J Polym Sci Polym Phys Ed* 31:2011
5. Phuong-Nguyen H, Delmas G (1992) *Macromolecules* 25:408
6. Phuong-Nguyen H, Delmas G (1992) *Macromolecules* 25:414
7. Zhang Z, Lapes I, Phuong-Nguyen H, Delmas G (1997) *Can J Chem* 75:1354
8. Phuong-Nguyen H, Delmas G (1995) *Collect Czech Chem Commun* 60:1905
9. Phuong-Nguyen H, Charlet G, Delmas G (1996) *J Thermal Anal* 46:809
10. Phuong-Nguyen H, Delmas G (1994) *J Solution Chem* 23:249
11. Phuong-Nguyen H, Delmas G (1994) *J Mater Sci* 29:3612
12. Le Lay P, Zhang X, Delmas G (1998) *Carbohydr polym* 37:49
13. Bernazzani P, Chapados C, Delmas G (2000) *J Polym Sci Polym Phys Ed* 38:1662
14. Bernazzani P, Bich VT, Phuong-Nguyen H, Haine A, Chapados C, Dao LH, Delmas G (1998) *Can J Chem* 76:1674
15. Bernazzani P (1995) MSc. Thesis, University of Quebec in Montreal
16. Haine A (1995) MSc thesis, Uqam, 1995 and not published work
17. Bernazzani P, Chapados C, Delmas G (2000) *Biopolymers* 58:305
18. Wunderlich B (1980) In: *Macromolecular physics*, vol 3. Academic press, London, p 12
19. Boyer RF, Miller RL (1987) In: Keinath SEM, Miller RL, Rieke JK (eds) *Order in the amorphous state of polymers*. Plenum Press, New York, p 135 and p 33
20. Brenner T, Rudin A (1992) *J Polym Sci Polym Phys Ed* 30:1247
21. Morin FG, Delmas G, Gilson D (1995) *Macromolecules* 28:3248
22. van Prooyen M, Brenner T and Rudin A (1992) report to the Institute for Polymer Research, University of Waterloo
23. Krugel JK (1979) *Solid State Commun* 30:43
24. Hussein A, Williams MC (2000) *Macromolecules* 33:520
25. Bent J, Hutchings LR, Richards RW, Gough T, Spares R, Coates PD, Grillo I, Harlen OG, Read DJ, Graham RS, Likhtman AE, Groves DJ, Nicholson TM, McLeish TCB (2003) *Sci: Int Edn – AAAS*. v.301, n.5640, p 1691, 5 p
26. Janimak JJ, Stevens GC (2001) *J Mater Sci* 36:1879
27. Wignall GD, Alamo RG, Ritchson EJ, Mandelkern L, Schwahn D (2001) *Macromolecules* 34:8160

28. Guichon O, Séguéla R, David L, Vigier GJ (2003) *J Polym Sci Polym Phys Ed* 41:327
29. Marigo A, Zannetti R, Milani F (1997) *Eur Polym J* 33:595
30. Jedidi I, Ferhat-Hamida Z, Delmas G (2007) *J Polym Sci Polym Phys Ed* 44:in revision
31. Barbalata A, Bohossian T, Prochaszka K, Delmas G (1988) *Macromolecules* 21:3286
32. Wedgewood AR, Seferis JC (1983) In: Seferis JC, Theocaris PS (eds) IUPAC publication
33. Agosti E, Zerbi G, Ward I (1993) *Polymer* 34:4219
34. Zerbi G, Gallino G, Del Fanti N, Baini L (1989) *Polymer* 30:2324
35. Painter PC, Havens J, Hart WW, Koenig JL (1977) *J Polym Sci Polym Phys Ed* 1237
36. Phuong-Nguyen H, Delmas G (1994) *Thermochimica Acta* 238:257
37. Pennings AJ, Smook S (1984) *J Mater Sci* 19:3443